A Linear Equivalent Circuit Model for Depletion-Type Silicon Microring Modulators

Myungjin Shin, Yoojin Ban, Byung-Min Yu, Min-Hyeong Kim, Jinsoo Rhim, *Student Member, IEEE*, Lars Zimmermann, and Woo-Young Choi, *Member, IEEE*

***Abstract*— We present a linear equivalent circuit model for the depletion-type Si microring modulator (MRM). Our model consists of three blocks: one for parasitic components due to interconnects and pads, one for the electrical elements of the core p-n junction, and the third for a lossy LC tank representing Si MRM optical modulation characteristics. Model parameter values are extracted from measurement of a fabricated Si MRM device. Simulated modulation characteristics with our equivalent circuit show very good agreement with measured results. Using our model, we can analyze Si MRM modulation frequency response characteristics and perform gain-bandwidth product optimization of the entire Si photonic transmitter composed of a Si MRM and electrical driver circuits.**

***Index Terms*— Equivalent circuit model, optical interconnect, silicon photonics, Si ring modulator.**

I. Introduction

Si PHOTONICS is attracting a great deal of research and development efforts, since it can provide cost-effective, high-bandwidth, and small-footprint optical interconnect solutions [1]. Among several photonic devices that can be used for Si photonic interconnect systems, the depletion-type Si microring modulator (MRM) is of special interest as it has large modulation bandwidth, a small footprint, and low-power consumption [2]–[7]. In designing optimal Si MRMs for target applications, a model that can accurately predict Si MRM modulation characteristics is very important. There have been several reports on Si MRM modulation characteristics analyses using either the time-dependent dynamics model [8] or the model based on the coupled-mode theory [9]–[15]. The time-dependent dynamics model provides very accurate results but using it can be computationally intensive. The model based on the coupled-mode theory is computationally less intensive, and its numerical solution has been implemented in Verilog-A [15], a popular behavior-level simulator among circuit designers. These numerical approaches, however, are not very convenient to use for design optimization.

In this paper, we introduce a linear equivalent circuit whose output voltage models the normalized output optical power of Si MRM in small-signal modulation condition. Although there have been several reports on the Si MRM circuit model [13]–[16], ours is the first model that can simulate both electrical and optical characteristics of the Si MRM entirely based on circuit parameters. In particular, using the circuit model for the Si MRM modulation characteristics, instead of scattering parameters or transfer functions within the circuit simulator, allows faster simulation, especially when designing integrated circuits containing several Si MRMs and electronic circuits. In addition, values of all our circuit parameters can be extracted in a straightforward way as will be demonstrated in this paper.

This paper is organized as follows. In Section II, we give details of our circuit model. In Section III, we explain how model parameter values are extracted from measurement. We also confirm the accuracy of our model by comparing Si MRM modulation characteristics simulated with the circuit model in Cadence Spectre, a very popular electrical circuit simulator, with measurement results. In Section IV, we demonstrate the usefulness of our model by analyzing the gain-bandwidth product of the entire Si photonic transmitter composed of a Si MRM and driver electronics. Section V concludes this paper.

II. Si MRM Equivalent Circuit Model

Fig. 1(a) and (b) shows the device structure and the cross section of a depletion-type Si MRM, respectively. The Si MRM device used for this paper has been fabricated through Si PIC MPW provided by IHP. The ring waveguide is divided into n- and p-regions with the nominal peak doping concentration of 7×10^{17} cm^{-3} for p-region and 3×10^{18} cm^{-3} for n-region.

Manuscript received August 16, 2016; revised November 25, 2016; accepted January 2, 2017. Date of publication January 27, 2017; date of current version February 24, 2017. This work was supported in part by the National Research Foundation of Korea through the Korean Ministry of Science, ICT, and Future Planning under Grant 2015R1A2A2A01007772 and in part by the Materials and Parts Technology Research and Development Program through the Korean Ministry of Trade, Industry & Energy under Project 10065666. The review of this paper was arranged by Editor E. G. Johnson.

M. Shin, B.-M. Yu, M.-H. Kim, and W.-Y. Choi are with the Department of Electrical and Electronic Engineering, Yonsei University, Seoul 03722, South Korea (e-mail: wchoi@yonsei.ac.kr).

Y. Ban was with the Department of Electrical and Electronic Engineering, Yonsei University, Seoul 03722, South Korea. She is now with imec, B-3001 Leuven, Belgium.

J. Rhim was with the Department of Electrical and Electronic Engineering, Yonsei University, Seoul 03722, South Korea. He is now with Hewlett Packard Laboratories, Palo Alto, CA 94304 Jinsoo USA.

L. Zimmermann is with Innovations for High Performance Microelectronics, 15236 Frankfurt, Germany.

Color versions of one or more of the figures in this paper are available online at http://ieeexplore.ieee.org.

Digital Object Identifier 10.1109/TED.2017.2648861

0018-9383 © 2017 IEEE. Personal use is permitted, but republication/redistribution requires IEEE permission.
See http://www.ieee.org/publications_standards/publications/rights/index.html for more information.

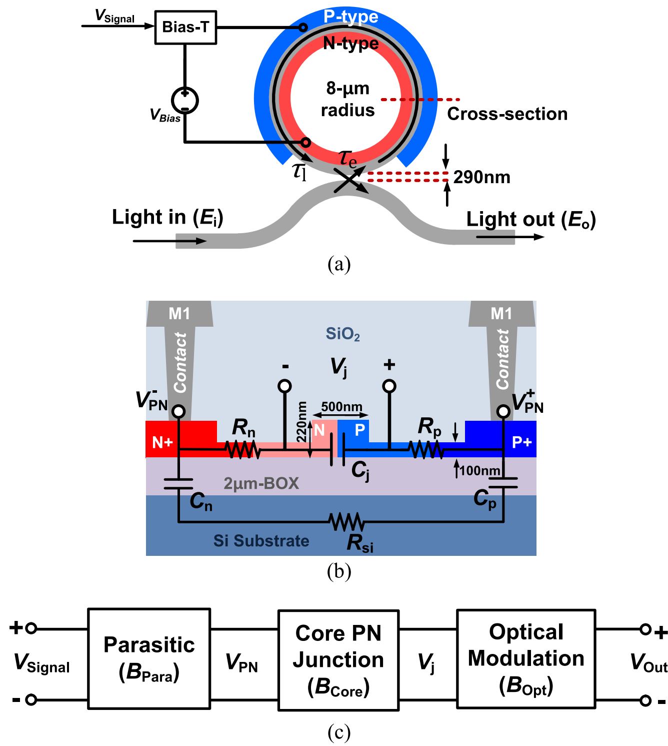

Fig. 1. (a) Structure, (b) cross section, and core electrical model of Si MRM. (c) Block diagram of Si MRM equivalent circuit.

The nominal width ratio is 2:3 for n- and p-regions. Similar devices having different doping concentrations have been used for parametric characterization of Si MRM self-heating [17]. In a depletion-type Si MRM, its p-n junction reverse bias voltage is modulated by external voltage signals, which causes the effective index modulation for the ring waveguide [18]. With this, the Si MRM resonance wavelength shifts and the amount of light coupled into the optical output port is modulated. The device can be modeled with three blocks, as shown in Fig. 1(c): B_{Para} for parasitic components for pads and interconnects, B_{Core} for electrical components of the Si MRM core, and B_{Opt} for a lossy LC tank, representing small-signal optical modulation characteristics of Si MRM. Detailed explanations for each block are given as follows.

A. B_{Para}: Pads and Interconnects

In previously reported models for Si MRMs, the influence of pads and interconnects has been considered together with the Si MRM core and simply modeled by one capacitor [14]–[16]. However, as the modulation speed increases, the effect of these parasitic components becomes more significant and providing an accurate model for them becomes necessary. Fig. 2(a) shows the parasitic components that should be considered. C_{pad} is the capacitance between two signal pads as well as metallic interconnects lines, and C_{ox1} and C_{ox2} are the capacitance between pad and silicon substrate for n-port and p-port, respectively. R_{sub} is the resistance through the silicon substrate between n-port and p-port pads through C_{ox1} and C_{ox2}. L_{int1}, L_{int2}, R_{int1}, and R_{int2} are inductances and resistances of interconnect lines for n-port and p-port terminals. $C_{\text{c-c}}$ represents the capacitance between two metal openings

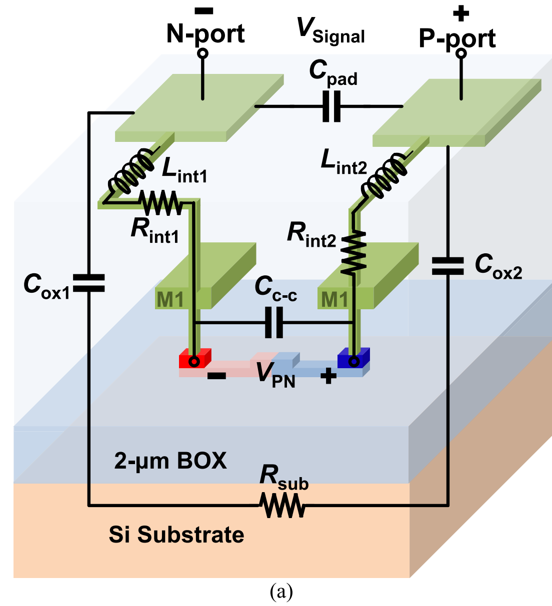

Fig. 2. (a) Parasitic components for pads and interconnects and (b) their equivalent circuit (B_{Para}).

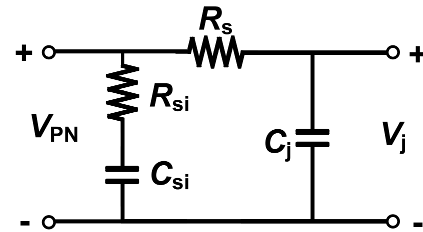

Fig. 3. Equivalent circuit for Si MRM Core (B_{Core}).

to n^+ and p^+ regions. The output voltage of this block is the voltage across the Si MRM p-n junction ($V_{\text{p-n}}$). Since the same amount of current flows in both n-port and p-port interconnect lines in this two-terminal device, we can simplify the circuit by using $C_{\text{ox}} = C_{\text{ox1}}||C_{\text{ox2}}, L_{\text{int}} = L_{\text{int1}} + L_{\text{int2}}$, and $R_{\text{int}} = R_{\text{int1}} + R_{\text{int2}}$. Fig. 2(b) shows the resulting equivalent circuit for B_{Para}.

B. B_{Core}: Si MRM Core

As shown in Fig. 1(b), the Si MRM core can be modeled with RC components [14]–[16]. C_j represents the junction capacitance for p-n junction, R_n and R_p represent the resistances in the doped Si layers, C_n and C_p represent the capacitance between doped silicon layers and the silicon substrate, and R_{si} represents the resistance of the silicon substrate below the device. Fig. 3 shows the equivalent circuit of the Si MRM

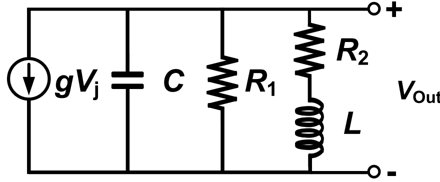

Fig. 4. Equivalent circuit for Si MRM optical modulation characteristics (B_{Opt}).

core where $R_s = R_n + R_p$ and $C_{\mathrm{si}} = C_n||C_p$. The output signal of this block is the voltage across C_j, since light in the Si MRM is modulated by the effective index variation due to the junction voltage (V_j) variation.

C. B_{Opt}: Optical Modulation Characteristics

When the Si MRM is modulated with a small-signal junction voltage given as $V_j(t) = v_0\cos(\omega_{\mathrm{m}}t)$ around the bias voltage, the change in the effective index with time, $\eta(t)$, can be expressed as

$$\eta(t) = \frac{\partial \eta}{\partial V_j} v_0 \cos(\omega_m t). \tag{1}$$

Considering only the linear response, the output optical signal is also modulated with the same angular frequency ω_m. The modulated optical signal is detected by a photodetector, generating photocurrents that are proportional to output optical power, P_{out}, of the Si MRM. This process can be modeled in the s-domain based on the coupled-mode equation as [11], [12]

$$\begin{aligned}\Delta_O(s) &= \frac{P_{\mathrm{out}}/P_{\mathrm{in}}(s)}{V_j(s)}\\ &= \frac{4}{\eta_0}\cdot\frac{\partial \eta}{\partial V_j}\cdot\frac{\omega_r D/\tau_e}{D^2+1/\tau^2}\cdot\frac{s+2/\tau_l}{s^2+(2/\tau)s+D^2+1/\tau^2}\end{aligned} \tag{2}$$

where $D(=|\omega_{\mathrm{in}}-\omega_{\mathrm{r}}|)$, the detuning parameter, represents how much the input light angular frequency ω_{in} is detuned from the ring resonance angular frequency ω_r, and and η_0 represent the effective index of the ring waveguide at the given bias voltage. τ_l and τ_e are decay time constants of the ring resonator due to the round-trip loss and ring-bus coupling, respectively. They satisfy $1/\tau_l + 1/\tau_e = 1/\tau$, where τ is the total decay time constant for the ring resonator. Equation (2) represents a two-pole and one-zero linear system whose damping factor ζ and natural frequency ω_n are given as $\zeta = (1/((1+D^2\tau^2)^{1/2}))$ and $\omega_n = (D^2+(1/\tau^2))^{1/2}$. Since ζ is smaller than 1 unless $D = 0$, the Si MRM has the underdamped modulation frequency response except at the resonance frequency.

Fig. 4 shows B_{Opt} that models the transfer function given in (2), where V_{out} represents normalized output power ($P_{\mathrm{out}}/P_{\mathrm{in}}$). It is composed of a lossy LC tank with a voltage-controlled current source having transconductance g and two additional resistors, R_1 and R_2. The transfer function for this circuit is given as

$$\Delta_E(s) = \frac{V_{\mathrm{Out}}(s)}{V_j(s)} = \frac{g}{C}\frac{s+\frac{R_2}{L}}{s^2+\left(\frac{1}{CR_1}+\frac{R_2}{L}\right)s+\frac{1}{LC}\left(\frac{R_2}{R_1}+1\right)}. \tag{3}$$

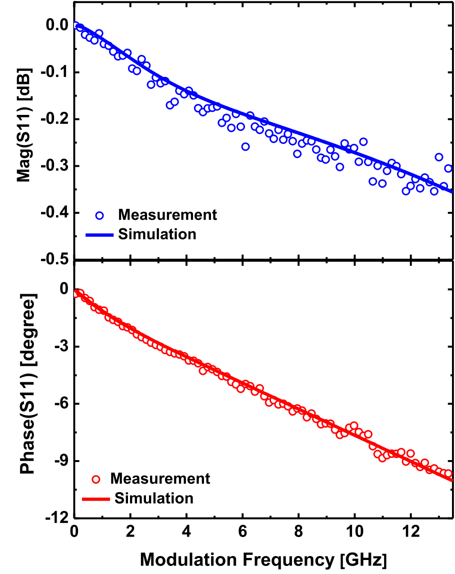

Fig. 5. Measured (circles) and simulated (colored solid lines) S_{11} of Si MRM at $V_{\mathrm{Bias}} = -1$ V.

By comparing (2) and (3), we can express circuit parameters in terms of τ_e, τ_l, and D as

$$R_1 C = \frac{\tau_e}{2} \tag{4}$$

$$\frac{L}{R_2} = \frac{\tau_l}{2} \tag{5}$$

$$\frac{R_1}{R_2} = [(1/\tau^2 + D^2)\tau_e\tau_l/4 - 1] \tag{6}$$

and

$$g = \frac{2}{\eta_0}\cdot\frac{\delta\eta}{\delta v}\cdot\frac{\omega_r D}{D^2+1/\tau^2}\frac{1}{R_1}U. \tag{7}$$

The unit conversion factor $U(=1\ \mathrm{V})$ is added in (7), so that g can have the correct unit of transconductance. Our model preserves the physical meaning of the two time constants of the ring resonator by representing τ_e with R_1C and τ_l with L/R_2. The factor of two shows up in (4) and (5), because τ_e and τ_l are time constants for electrical fields whereas the equivalent circuit models the optical power. Damping factor ζ and natural frequency ω_n are given as $\zeta = (CR_1R_2 + L)/(2(LCR_1(R_1+R_2))^{1/2})$ and

$$\omega_n = \sqrt{\frac{1}{LC}\left(\frac{R_2}{R_1}+1\right)} = ((1/(LC))((R_2/R_1)+1))^{\frac{1}{2}}.$$

III. Parameter Value Extraction and Model Verification

B_{Para} can be determined from electrical S_{11} measurement of short and open test patterns having the same pad and interconnect structures as the target Si MRM fabricated on the same die [19]. In this paper, open and short test patterns have the same structure from pad to Metal 1. Since neither short nor open test pattern includes $C_{\text{c-c}}$, we first determined

TABLE I
EXTRACTED PARAMETER VALUES FOR B_{PARA} AND B_{CORE}

C_{pad}	4.9 fF
C_{OX}	5.8 fF
R_{sub}	3.893 KΩ
L_{int}	108 pH
R_{int}	1.1 Ω
$C_{c\text{-}c}$	5 fF
R_{si}	23 KΩ
C_{si}	7 fF
R_s	365.5 Ω
C_j	8.2 fF

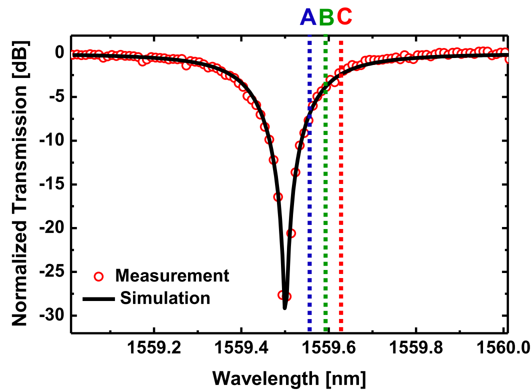

Fig. 6. Measured and simulated transmission characteristics of Si MRM at $V_{Bias} = -1$ V.

the value of $C_{c\text{-}c}$ by EM simulation. Then, by fitting simulated S_{11} values to measured results, we can determine the numerical value for each component in B_{Para}, as shown in Table I. With B_{Para} known, B_{Core} can be determined by fitting simulated S_{11} values for B_{Para} and B_{Core} into measured values. Fig. 5 shows the magnitude and phase response of measured (circles) and simulated (colored solid lines) S_{11} values at $V_{Bias} = -1$ V with extracted parameter values listed in Table I.

For B_{Opt}, values for L, C, R_1, and R_2 can be determined from τ_e, τ_l, and D using (4)–(6). With the knowledge of R_1 value, g can be determined from optical parameters, η_0, D, ω_r, τ, and $\delta\eta/\delta v$. For determination of η_0, the ring resonance mode number m can be first identified as 85 from waveguide simulation of the Si MRM. With this, η_0 can be determined as 2.637149 at $V_{Bias} = -1$ V from the resonance condition $m\lambda_{res} = L\eta_0$ with measured λ_{res}. The value of τ_e and τ_l, can be determined by fitting the Si MRM steady-state transmission characteristic given as [20], [21]

$$T = \frac{P_{out}}{P_{in}} = \left| \frac{j\omega - j\omega_r + 1/\tau_l - 1/\tau_e}{j\omega - j\omega_r + 1/\tau_l + 1/\tau_e} \right|^2. \quad (8)$$

to the measured transmission characteristics, as shown in Fig. 6, at $V_{Bias} = -1$ V with the minimum mean squared error [22].

TABLE II
B_{OPT} PARAMETER VALUES

$D=\|\omega_{in}-\omega_{res}\|$ ($\|\lambda_{in}-\lambda_{res}\|$)	(A) 50.3 RAD/S (65pm)	(B) 73.6 RAD/S (95pm)	(C) 96.8 RAD/S (125pm)
g (A/V)	2.93x10^{-5}	1.55x10^{-5}	8.95x10^{-6}
R_1 (KΩ)	3.585	7.642	13.221
R_2 (KΩ)		10	
C (fF)	3.4356	1.6116	0.9316
L (nH)		114.413	

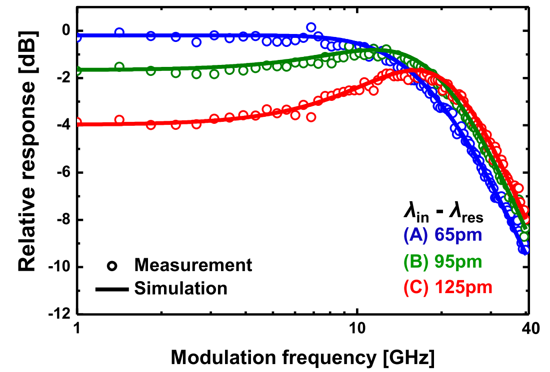

Fig. 7. Measured (circles) and simulated (solid lines) relative frequency responses at three different detuning values ($V_{Bias} = -1$ V).

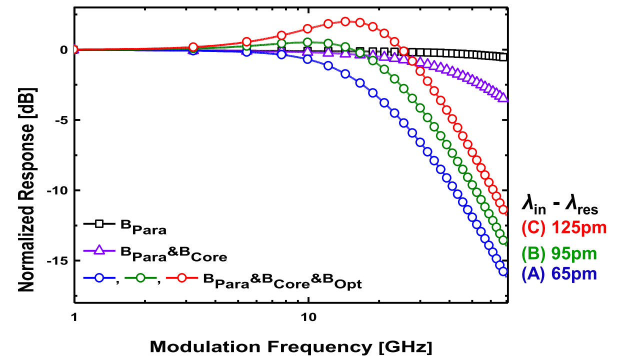

Fig. 8. Simulated normalized frequency responses of B_{Para}, B_{Para}, and B_{Core}, and B_{Para}, B_{Core}, and B_{Opt} at three different detuning values.

For this measure, input optical power after the grating coupler is minimized to −15 dBm in order to avoid any self-heating. With this fitting, $\tau_e = 24.635$ ps and $\tau_l = 22.882$ ps are determined. The value for g can be determined from (7) using the measured value of $\delta\eta/\delta v$ of 2.2×10^{-5} at $V_{Bias} = -1$ V. The corresponding B_{Opt} circuit parameter values at three different detuning values are listed in Table II, where R_2 is fixed at 10 kΩ for convenience.

The simulated Si MRM modulation frequency responses at $V_{Bias} = -1$ V for three different detuning values are shown in Fig. 7 along with the measured results. Both simulation and measured results are normalized to the low-frequency value of case (A). The simulation is done with Cadence Spectre (Virtuoso Version No. 14.1.0.459), using circuit parameters

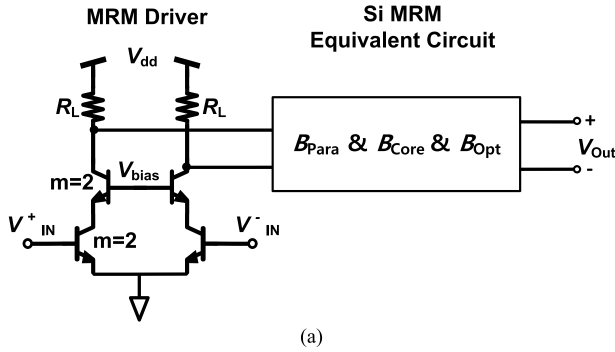

(a)

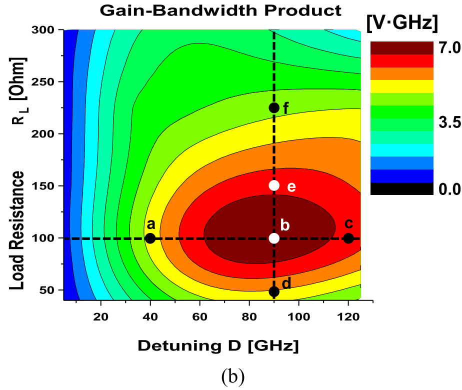

(b)

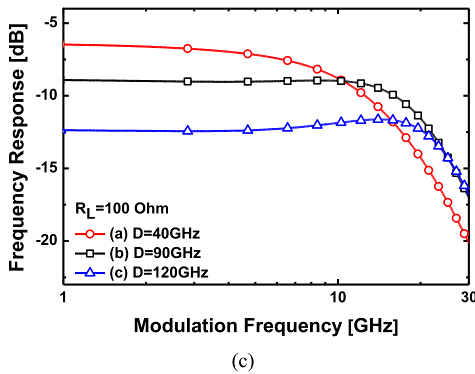

(c)

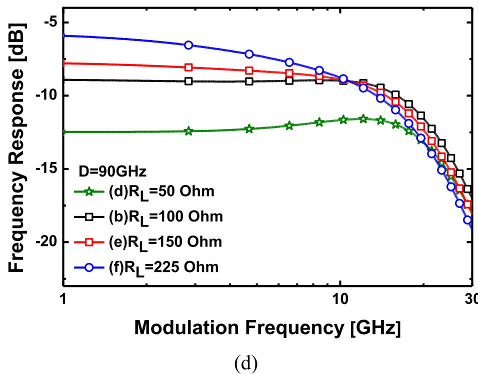

(d)

Fig. 9. (a) Schematic of Si MRM transmitter. (b) Simulated gain-bandwidth product of the transmitter with different driver load impedance (R_L) and D values. Simulated transmitter frequency responses at (c) three different detuning values with $R_L = 100\ \Omega$ and (d) four different R_L values with $D = 90$ GHz.

values given in Tables I and II. Clearly, different modulation frequency responses of Si MRM at different detuning conditions are accurately modeled with our equivalent circuit.

IV. Application of the Equivalent Circuit

Using our model, we can identify how much each of B_{para}, B_{Core}, and B_{Opt} contributes to the modulation frequency response. Fig. 8 shows the simulated normalized modulation frequency responses for only parasitic components (B_{Para}), including parasitic and core components (B_{Para} and B_{Core}), and full equivalent circuit model (B_{Para}, B_{Core}, and B_{Opt}) for three different detuning conditions. For the Si MRM device under investigation, the 3-dB modulation bandwidth due to electrical components is approximately 65 GHz, and consequently, the modulation frequency response is mainly limited by B_{Opt}. It is possible to enlarge the bandwidth of B_{Opt} by reducing Q-factor of the ring resonator, or by designing a Si MRM having lower value for τ but at the cost of reduced modulation gain as can be seen in (7).

The real advantage of the Si MRM equivalent circuit is the ease with which it can be used for cosimulation of electronic circuits and Si MRMs in a similar manner as has been demonstrated for Mach–Zehnder modulators and electroabsorption modulators [23], [24]. Fig. 9(a) shows a schematic for an integrated Si photonic transmitter based on a pseudodifferential cascode common-emitter driver and a Si MRM. Such an integrated circuit can be fabricated with IHP's EPIC technology, which provides monolithic integration of 0.25-μm SiGe BiCMOS and Si PIC technologies [25]. In this transmitter, the value of load resistance R_L should be carefully optimized. Fig. 9(b) shows the simulated gain-bandwidth products as a function of R_L and D. Simulated frequency responses for selected points are shown in Fig. 9(c) for different D values and in Fig. 9(d) for different R_L values. Clearly, the gain-bandwidth product is a sensitive function of electrical characteristics represented by R_L and optical characteristics represented by D, and our Si MRM circuit model allows its optimization in a very straightforward manner.

V. Conclusion

We presented an equivalent circuit model for the depletion-type Si MRM. The model has three blocks, each of which models parasitic components, core Si MRM p-n junction, and the modulation characteristics of the Si MRM. The circuit model parameters are extracted from relatively simple device measurement and simulation. The accuracy of our model is confirmed by measurement. Our circuit model allows efficient cosimulation of Si MRMs with electronic circuits in the standard electronic circuit simulation environment, which should be of great help for efficient design of Si electronic-photonic integrated circuits containing Si MRMs.

References

[1] R. Soref, "The past, present, and future of silicon photonics," *IEEE J. Sel. Topics Quantum Electron.*, vol. 12, no. 6, pp. 1678–1687, Nov./Dec. 2006.

[2] P. Dong *et al.*, "Low V_{pp}, ultralow-energy, compact, high-speed silicon electro-optic modulator," *Opt. Exp.*, vol. 17, no. 25, pp. 22484–22490, 2009.

[3] G. Li *et al.*, "Ring resonator modulators in silicon for interchip photonic links," *IEEE J. Sel. Topics Quantum Electron.*, vol. 19, no. 6, Nov./Dec. 2013, Art. no. 3401819.

[4] X. Xiao *et al.*, “44-Gb/s silicon microring modulators based on zigzag PN junctions,” *IEEE Photon. Technol. Lett.*, vol. 24, no. 19, pp. 1712–1714, Oct. 1, 2012.
[5] M. Pantouvaki *et al.*, “50Gb/s silicon photonics platform for short-reach optical interconnects,” in *Proc. Opt. Fiber Commun. Conf. (OFC)*, 2016, p. Th4H.4.
[6] M. Pantouvaki, P. Verheyen, J. De Coster, G. Lepage, P. Absil, and J. Van Campenhout, “56Gb/s ring modulator on a 300mm silicon photonics platform,” in *Proc. IEEE Eur. Conf. Opt. Commun. (ECOC)*, Sep./Oct. 2015, pp. 1–3.
[7] X. Xiao *et al.*, “60 Gbit/s silicon modulators with enhanced electro-optical efficiency,” in *Proc. Opt. Fiber Commun. Conf./Nat. Fiber Opt. Eng. Conf. (OFC/NFOEC)*, 2013, p. OW4J.3.
[8] W. D. Sacher and J. K. S. Poon, “Dynamics of microring resonator modulators,” *Opt. Exp.*, vol. 16, no. 20, pp. 15741–15753, 2008.
[9] L. Zhang, Y. Li, J.-Y. Yang, M. Song, R. G. Beausoleil, and A. E. Willner, “Silicon-based microring resonator modulators for intensity modulation,” *IEEE J. Sel. Topics Quantum Electron.*, vol. 16, no. 1, pp. 149–158, Jan./Feb. 2010.
[10] M. Song, L. Zhang, R. G. Beausoleil, and A. E. Willner, “Nonlinear distortion in a silicon microring-based electro-optic modulator for analog optical links,” *IEEE J. Sel. Topics Quantum Electron.*, vol. 16, no. 1, pp. 185–191, Jan. 2010.
[11] B. Pile and G. Taylor, “Small-signal analysis of microring resonator modulators,” *Opt. Exp.*, vol. 22, no. 12, pp. 14913–14928, 2014.
[12] Y. Ban, J.-M. Lee, B.-M. Yu, S.-H. Cho, and W.-Y. Choi, “Small-signal frequency responses for Si micro-ring modulators,” in *Proc. IEEE Opt. Interconnects Conf.*, May 2014, pp. 47–48.
[13] J. Müller *et al.*, “Optical peaking enhancement in high-speed ring modulators,” *Sci. Rep.*, vol. 4, Aug. 2014, Art. no. 6310.
[14] S. Karimelahi and A. Sheikholeslami, “Ring modulator small-signal response analysis based on pole-zero representation,” *Opt. Exp.*, vol. 24, no. 7, pp. 7585–7599, 2016.
[15] J. Rhim, Y. Ban, B.-M. Yu, J.-M. Lee, and W.-Y. Choi, “Verilog-A behavioral model for resonance-modulated silicon micro-ring modulator,” *Opt. Exp.*, vol. 23, no. 7, pp. 8762–8772, 2015.
[16] G. Li *et al.*, “25Gb/s 1V-driving CMOS ring modulator with integrated thermal tuning,” *Opt. Exp.*, vol. 19, no. 21, pp. 20435–20443, 2011.
[17] M. J. Shin, Y. Ban, B.-M. Yu, J. Rhim, L. Zimmermann, and W.-Y. Choi, “Parametric characterization of self-heating in depletion-type Si micro-ring modulators,” *IEEE J. Sel. Topics Quantum Electron.*, vol. 22, no. 6, Nov./Dec. 2016, Art. no. 3400207.
[18] R. A. Soref and B. R. Bennett, “Electrooptical effects in silicon,” *IEEE J. Quantum Electron.*, vol. 23, no. 1, pp. 123–129, Jan. 1987.
[19] A. Aktas and M. Ismail, “Pad de-embedding in RF CMOS,” *IEEE Circuits Devices Mag.*, vol. 17, no. 3, pp. 8–11, May 2001.
[20] H. A. Haus, “Coupling of modes-resonators and couplers,” in *Waves and Fields in Optoelectronics*. Englewood Cliffs, NJ, USA: Prentice-Hall, 1984, p. 07632.
[21] B. E. Little, S. T. Chu, H. A. Haus, J. S. Foresi, and J.-P. Laine, “Microring resonator channel dropping filters,” *J. Lightw. Technol.*, vol. 15, no. 6, pp. 998–1005, Jun. 1997.
[22] B.-M. Yu, J.-M. Lee, Y. Ban, S.-H. Cho and W.-Y. Choi, “Model parameter extraction for Si micro-ring modulator,” in *Proc. OECC/ACOFT*, 2014, pp. 830–831.
[23] M. Pirola, F. Cappelluti, G. Giarola, and G. Ghione, “Multisectional modeling of high-speed electrooptic modulators integrated in a microwave circuit CAD environment,” *J. Lightw. Technol.*, vol. 21, no. 12, pp. 2989–2996, Dec. 2003.
[24] F. Cappelluti, A. Mela, M. Pirola, and G. Ghione, “Large-signal E/O modelling of traveling-wave electroabsorption modulators in an RF circuit CAD environment,” in *IEEE MTT-S Int. Microw. Symp. Dig.*, Jun. 2004, pp. 769–772, paper WE3C-3.
[25] L. Zimmermann *et al.*, “Monolithically integrated 10Gbit/sec silicon modulator with driver in 0.25[micro]m SiGe:C BiCMOS,” in *Proc. Eur. Conf. Exhibit. Opt. Commun. (ECOC)*, 2013, p. We.3.B.1.

Myungjin Shin is currently pursuing the M.S. degree with Yonsei University, Seoul, South Korea.

His current research interests include design, modeling, and optimization of Si microring modulators.

Yoojin Ban received the M.S. degree from Yonsei University, Seoul, South Korea, in 2015.

She joined imec, Leuven, Belgium, where she is currently involved in high-performance Si modulators.

Byung-Min Yu is currently pursuing the Ph.D. degree with Yonsei University, Seoul, South Korea.

His current research interests include design, modeling, and optimization of silicon photonic devices.

Min-Hyeong Kim is currently pursuing the Ph.D. degree with Yonsei University, Seoul, South Korea.

His current research interests include high-speed interface circuits for optical interconnects.

Jinsoo Rhim (S’17) received the Ph.D. degree from Yonsei University, Seoul, South Korea, in 2016.

He joined Hewlett Packard Laboratories, Palo Alto, CA, USA. His current research interests include photonic device characterization and modeling, Si-based electronic-photonic IC design, and high-speed interface circuit design in advanced CMOS/BiCMOS technology.

Lars Zimmermann received the Ph.D. degree in electrical engineering from Katholieke Universiteit Leuven, Leuven, Belgium, focused on near-infrared sensor arrays, which he conducted at IMEC.

He was with IHP, Frankfurt (Oder), Germany, in 2008. He is currently a Team Leader with Silicon Photonics Technologies, California, USA. He is also with TU Berlin, Berlin, Germany, coordinating the cooperation with IHP in the field of Si photonics.

Woo-Young Choi (M’92) received the B.S., M.S., and Ph.D. degrees in electrical engineering and computer science from the Massachusetts Institute of Technology, Cambridge, MA, USA, focused on molecular-beam epitaxy-grown InGaAlAs laser diode.

He is currently a Professor of Electrical and Electronic Engineering, Yonsei University, Seoul, Korea. His current research interests include high-speed circuits and systems, that are Si photonics and high-speed Si integrated circuits for interface applications.